South African speleothems reveal influence of high- and lowlatitude forcing over the past 113.5 k.y.

Brian M. Chase, Chris Harris, Maarten de Wit, Jan Kramers, Sean Doel, Jacek Stankiewicz

South African speleothems reveal influence of high- and low-latitude forcing over the last 113.5 kyr

Brian Chase[1,2], Chris Harris[3], Maarten J de Wit[4], Jan Kramers[5], Sean Doel[3,6] and Jacek Stankiewicz[7]

[1]*Institut des Sciences de l'Evolution-Montpellier (ISEM), University of Montpellier, Centre National de la Recherche Scientifique (CNRS), EPHE, IRD, 34095 Montpellier, France*

[2]*Department of Environmental and Geographical Science, University of Cape Town, South Lane, Upper Campus, 7701 Rondebosch, South Africa*

[3]*Department of Geological Sciences, University of Cape Town, 7700 Rondebosch, South Africa*

[4]*AEON & Earth Stewardship Science Research Institute, Nelson Mandela University, 6031 Port Elizabeth, South Africa*

[5]*Department of Geology, University of Johannesburg, 2006 Johannesburg, South Africa*

[6]*WSP, Environment & Energy, 8001 Cape Town, South Africa*

[7]*European Center for Geodynamics and Seismology, Rue Josy Welter, 19 L-7256 Walferdange, Luxembourg*

ABSTRACT

Variation in $\delta^{18}O$ and $\delta^{13}C$ values in a speleothem from the Cango Caves in southernmost South Africa enable the construction of coherent regional composite records spanning the last 113,500 years. Novel for the region in terms of both their length and detail, these records indicate environmental and climatic changes that are both consistent with records from the wider region and show a clear evolution from low- to high latitude forcing dominance across the last glacial period. Prior to ~70 ka, the influence of direct low latitude insolation forcing is expressed through increases in summer rainfall during austral summer insolation maxima. With the onset of Marine Isotope Stage 4, cooler global conditions and the development of high latitude ice sheets appear to have supplanted direct insolation forcing as the dominant driver pacing patterns of environmental change, with records from the Southern and Northern Hemisphere tropics exhibiting a positive relationship until after the Last Glacial Maximum. These results highlight the complexity of South African climate change dynamics as a response to changing global boundary conditions and provide a critical reference for regional and global comparisons.

INTRODUCTION

Terrestrial proxy records of past environmental change in southern Africa are spatially and temporally restricted. The region's semi-arid to arid climates do not favour the development of natural lakes and wetlands, and long, continuous terrestrial palaeoenvironmental records are rare (see review by Chase and Meadows, 2007). This fundamental limitation becomes increasingly acute with age, with few records spanning Marine Isotope Stages (MIS) 3-5. As a result, little is known about climate and environmental dynamics in South Africa during the last glacial period. Existing records indicate the transient dominance of both 1) direct low-latitude orbital forcing (Partridge et al., 1997) and 2) high northern latitudes forcing, as transmitted to southern Africa via atmospheric and oceanic teleconnections (Chase et al., 2015; Chevalier and Chase, 2015; Schefuß et al., 2011). Lacking, however, is a basis to study how regional climates and environments responded to the changing global boundary conditions that were associated with the transition from interglacial to glacial climates. This is a period is of particular importance in South Africa because it represents a crucial time for human cultural and technological evolution, including the Still Bay and Howiesons Poort industries (Jacobs et al., 2008). To date, without sufficiently detailed, reliable records, it has not been possible to establish a firm link between these episodes and potential environmental forcing factors.

In this paper, we address this issue with the oxygen and carbon isotope stratigraphy of a 1.5 m stalagmite from the Cango Caves (Fig. 1, SI1), a cave site that has provided seminal records that have been fundamental to our understanding of southern African palaeoenvironments (Talma and Vogel, 1992). Encompassing the period from 40.1-106 ka, we use $\delta^{18}O$ and $\delta^{13}C$ records from the stalagmite as lynchpins to use reduced major axis (RMA) regression to establish regional composite records (Fig. 2) including previously published data from the site (Talma and Vogel, 1992), data from the nearby site of Efflux Cave (Braun et al., 2020) and – for $\delta^{13}C$ – rock hyrax middens from Seweweekspoort (Chase et al., 2017) (Fig. 1) (for further information regarding materials, methods and results supporting the details and discussion provided here, please refer to the Supplementary Information). These composite $\delta^{18}O$ and $\delta^{13}C$ records span the last 113.5 kyr and are used to explore the nature and dynamics of environmental change and its drivers across the last interglacial-glacial transition and last glacial cycle.

REGIONAL SETTING

The Cango Caves (Fig. 1, SI1) form a string of interconnected sub-horizontal linear caverns, some 2.5 km long, within deformed Proterozoic limestone of the Groot Swartberg Mountains of South Africa. The cave system is formed below a Cretaceous-Cenozoic paleo-denudation surface. The vegetation at Cango Caves is Kango Limestone Renosterveld (Rebelo et al., 2006), a grassy shrubland dominated by renosterbos (*Elytropappus rhinocerotis*) and shrubs and grasses of both C_3 and C_4 varieties (Vogel, 1978). Crassulacean Acid Metabolism (CAM) plants (many succulents) including *Aloe* spp. and succulent shrubs (particularly Crassulaceae) can be abundant in the region. Climate in South Africa is broadly determined by two dominant climate systems, the tropical easterlies which advect moist air off the warm southwestern Indian Ocean during the summer months, and frontal systems embedded in the westerly storm track that bring rain to the southwestern Cape and southern Cape coast during the winter months (Tyson, 1986) (Fig. 1). Spatial distinctions in rainfall regimes across the subcontinent have given rise to the classification of a winter rainfall zone (WRZ), an aseasonal or year-round rainfall zone (ARZ or YRZ) and a summer rainfall zone (SRZ) (sensu Chase and Meadows, 2007). The Cango Caves are located in the modern ARZ, receiving ~48% of its mean annual rainfall in the winter months (MJJAS) (Hijmans et al., 2005).

DISCUSSION

In general, variability in speleothem calcite $\delta^{18}O$ values ($\delta^{18}O_c$) is controlled by cave temperature and the $\delta^{18}O$ of the rainwater percolating into the cave. Rainwater $\delta^{18}O$ values ($\delta^{18}O_p$) are governed by a series of inter-related ‘effects’ (Dansgaard, 1964), namely temperature, source, continentality and the “amount effect”, the latter of which is particularly significant in tropical regions, such as South Africa’s summer rainfall zone (Herrmann et al., 2017). In South Africa’s winter rainfall zone, lower $\delta^{18}O_p$ is associated with cooler, wetter winter months and stratiform rainfall (Aggarwal et al., 2016; Harris et al., 2010; IAEA/WMO, 2020). Considering South Africa’s position – and particularly that of the study region – at the dynamic interface between tropical and temperate climate regimes (Chase et al., 2017; Chevalier and Chase, 2015; Schefuß et al., 2011), each of these effects and factors are likely to have influenced regional $\delta^{18}O_c$ records, and parsing them – and the influence of other effects - to isolate distinct controls has proven to be generally intractable (see Holmgren et al., 2003) particularly over the time periods considered here.

Variability in speleothem calcite $\delta^{13}C$ ($\delta^{13}C_c$) primarily reflects changes in the aggregate $\delta^{13}C$ value of the soil organics (Fohlmeister et al., 2020), which in turn depends primarily on the plant’s photosynthetic pathway (C_3,~-34 to -24‰; C_4,~-16 to -10‰ and CAM, ~-20 to -10‰) (O'Leary, 1988; Smith and Epstein, 1971). Of these, C_3 plants are generally trees and shrubs as well as grasses that grow in cool to cold environments, C_4 plants are primarily grasses adapted to warm growing seasons, and CAM represents an adaptation to water stress. As mentioned, plants of each type currently exist in the study region, and their proportions have been demonstrated to vary in the past as a function of changing climate (Sealy et al., 2016). Other factors, such as changes in vegetation density (and thus soil respiration), and prior carbonate precipitation are considered unlikely to have had significant influence on the $\delta^{13}C_c$ records as the nature of the regional vegetation types (Rebelo et al., 2006), the amplitude of regional temperature changes (Chase and Meadows, 2007), and the lack of correlation between $\delta^{13}C_c$ and speleothem growth rates (Fohlmeister et al., 2020) are not conducive to, or consistent with, significant variability related to such factors.

Across the last 113.5 kyr, the CFC $\delta^{13}C$ record highlights the influence of temperature on regional vegetation, with cooler global temperatures generally corresponding with less C_4 grass (Fig. 2). This relationship, however, evolves as a function of changing global boundary conditions. Prior to the onset of Marine Isotope Stage 4 (MIS 4) at ~70 ka, CFC $\delta^{13}C$ variability is consistent with orbital precession, with the most compelling comparison existing with the precipitation reconstruction from Tswaing Crater (Fig. 1, 2). Located ~1000 km to the northeast of the Cango Caves in the summer rainfall zone, the Tswaing Crater record has been presented as evidence for the influence of direct insolation forcing in southern Africa (Partridge et al., 1997), and the CFC $\delta^{13}C$ record indicates increases in C_4 grass prevalence during periods of increased summer rainfall.

The CFC $\delta^{13}C$ record provides corroboration for the results and interpretation of the Tswaing Crater record and together they enable a more reliable basis for comparison with other records from further afield. Of particular interest are records from the Northern Hemisphere tropics that can be used to assess the nature and dynamics of direct precessional forcing since the eccentricity maximum at 115 ka (Laskar et al., 2004). Of these, a δD record from leaf waxes from marine core RC09-166 in the Gulf of Aden (Tierney et al., 2017) provides the clearest reflection of northeast African tropical hydroclimate over this time period. Consistent with predictions based on direct precession-paced insolation forcing (Partridge et al., 1997), the period from 115 ka to ~70 ka is characterized by an antiphase relationship between patterns of precipitation change in the northeastern and southeastern African tropics (Fig. 2e). However, with declining eccentricity the negative correlation between Northern and Southern Hemisphere records diminishes with the onset of MIS 4. From ~70 ka to the beginning of the Holocene, Tswaing Crater and the Gulf of Aden record exhibit a strong positive correlation at precessional timescales, indicating a dominant influence of Northern Hemisphere high latitude forcing throughout this period (Fig. 2e). The change in CFC $\delta^{13}C$ likely reflects a change from summer to winter rainfall dominance in the Cango region. The more progressive nature of the change in relationship between the CFC $\delta^{13}C$ record and the northern tropics may reflect the influence of cooler temperatures on regional vegetation following the onset of MIS 4 or a dynamic specific to changes in summer vs. winter rainfall regimes at the distal margin of the summer rainfall zone (Fig.1).

The trend from low- to high latitude dominance is also evident in the comparison of the CFC $\delta^{18}O_c$ record and the composite $\delta^{18}O_c$ record from Chinese speleothems reflecting Asian monsoon dynamics and the impact of global climate change on low northern latitudes (Cheng et al., 2016). Highlighted again is a strong negative correlation prior to the onset of MIS 4, and a transition to a strong positive relationship with the shift to high latitude dominance (Fig. 2). The timing and nature of CFC $\delta^{18}O_c$ anomalies prior to ~70 ka correlate well both with 1) increased summer insolation and precipitation at Tswaing Crater as well as 2) proxies for more extensive Antarctic sea-ice (Fischer et al., 2007) (Fig. 2), which may have displaced the westerlies storm track equatorward, resulting in increased winter rainfall in the region (Chase et al., 2017). However, coeval increases in CFC $\delta^{13}C_c$ (more C_4 grasses) indicate that these phases of lower CFC $\delta^{18}O_c$ are most likely the result of more/more regular summer rain (Fig. 2), and suggest limitations in interpretive models that ascribe lower $\delta^{18}O_c$ values to increased proportions of winter rain (Braun et al., 2020), as this would generally result in lower $\delta^{13}C$ values.

While CFC $\delta^{18}O$ variability after ~70 ka is consistent with variability in Greenland ice cores reflecting temperature variability during MIS 4-2 (Rasmussen et al., 2014)(Fig. 2), and the nature of the CFC $\delta^{18}O$ record during this period would be consistent with changes in cave temperature, extending this interpretation of Talma and Vogel (1992) (reconstructed by estimating the $\delta^{18}O$ of past precipitation using groundwater $\delta^{18}O$ values from the nearby Uitenhage Aquifer) cannot be reliably established without a more complete record of past precipitation $\delta^{18}O$. Other explanations could relate to an increase in the influence of winter rainfall associated with the strong increase in Antarctic sea-ice at the onset of MIS 3 (~57 ka) (Fischer et al., 2007)(Fig. 2) and a displacement of the frontal systems and predominantly stratiform rainfall (generally lower $\delta^{18}O_p$; Aggarwal et al., 2016) associated with the mid-latitude westerlies storm track. This would indicate a change from summer to winter rainfall dominance across MIS 4, but – as this relationship is not maintained after the onset of MIS 2 (~29 ka) – more work remains to be done to adequately contextualize and understand the long-term variability of - and influences on - $\delta^{18}O_c$ in the region.

The MIS 4 transition from low- to high latitude dominance is also concurrent with the Still Bay and Howiesons Poort lithic industries (Fig. 2). Finding no clear relationship with Antarctic temperature records, Jacobs et al. (2008) concluded these industries could not be explained by environmental factors alone. While not establishing a comprehensive case for how environment/climatic conditions acted as a driver of the Still Bay and Howiesons Poort, the CFC records do show that each industry is associated with episodes of environmental change, likely periods of cooler conditions with decreased summer rainfall (Fig. 2). The records presented here cannot on their own define the nature of the relationship between environmental and cultural change, but they do provide a much clearer framework within which more comprehensive models may be established.

CONCLUSIONS

New speleothem $\delta^{13}C$ and $\delta^{18}O$ records from the Cango Caves have enabled the construction of regional composite records that highlight important aspects of the evolution of South African climate across the last glacial period. Prior to ~70 ka, direct low latitude insolation forcing is the primary driver of orbital scale climate variability, as expressed by peaks in summer rainfall and the development of more extensive C_4 grass cover during phases of relative aridity in the Northern Hemisphere tropics (Fig. 2). After ~70 ka, under decreasing orbital eccentricity and with the development of more extensive high latitude ice sheets, high latitude forcing becomes the dominant driver of climate change, with strong positive relationships and a synchronous relationship being established between the Northern and Southern Hemisphere tropics at orbital timescales.

ACKNOWLEDGMENTS

We thank Hein Gerstner the Chief Scientific Officer of the Cango Caves for support in 1995, and the National Monuments Council for permission to remove the stalagmite. Fayrooza Rawoot helped with the C and O isotope analyses. This work was funded through various grants of the National Research Foundation (NRF) to MDW and CH. We would also like to thank the editor and two anonymous reviewers for their constructive suggestions.

REFERENCES CITED

Aggarwal, P. K., Romatschke, U., Araguas-Araguas, L., Belachew, D., Longstaffe, F. J., Berg, P., Schumacher, C., and Funk, A., 2016, Proportions of convective and stratiform precipitation revealed in water isotope ratios: Nature Geoscience, v. 9, no. 8, p. 624-629.

Bar-Matthews, M., Marean, C. W., Jacobs, Z., Karkanas, P., Fisher, E. C., Herries, A. I. R., Brown, K., Williams, H. M., Bernatchez, J., Ayalon, A., and Nilssen, P. J., 2010, A high resolution and continuous isotopic speleothem record of paleoclimate and paleoenvironment from 90 to 53 ka from Pinnacle Point on the south coast of South Africa: Quaternary Science Reviews, v. 29, no. 17-18, p. 2131-2145.

Braun, K., Bar-Matthews, M., Matthews, A., Ayalon, A., Cowling, R. M., Karkanas, P., Fisher, E. C., Dyez, K., Zilberman, T., and Marean, C. W., 2019, Late Pleistocene records of

speleothem stable isotopic compositions from Pinnacle Point on the South African south coast: Quaternary Research, v. 91, no. 1, p. 265-288.
Braun, K., Bar-Matthews, M., Matthews, A., Ayalon, A., Zilberman, T., Cowling, R. M., Fisher, E. C., Herries, A. I. R., Brink, J. S., and Marean, C. W., 2020, Comparison of climate and environment on the edge of the Palaeo-Agulhas Plain to the Little Karoo (South Africa) in Marine Isotope Stages 5–3 as indicated by speleothems: Quaternary Science Reviews, v. 235, p. 105803.
Chase, B. M., Boom, A., Carr, A. S., Carré, M., Chevalier, M., Meadows, M. E., Pedro, J. B., Stager, J. C., and Reimer, P. J., 2015, Evolving southwest African response to abrupt deglacial North Atlantic climate change events: Quaternary Science Reviews, v. 121, no. 0, p. 132-136.
Chase, B. M., Chevalier, M., Boom, A., and Carr, A. S., 2017, The dynamic relationship between temperate and tropical circulation systems across South Africa since the last glacial maximum: Quaternary Science Reviews, v. 174, p. 54-62.
Chase, B. M., and Meadows, M. E., 2007, Late Quaternary dynamics of southern Africa's winter rainfall zone: Earth-Science Reviews, v. 84, no. 3-4, p. 103-138.
Cheng, H., Edwards, R. L., Sinha, A., Spötl, C., Yi, L., Chen, S., Kelly, M., Kathayat, G., Wang, X., Li, X., Kong, X., Wang, Y., Ning, Y., and Zhang, H., 2016, The Asian monsoon over the past 640,000 years and ice age terminations: Nature, v. 534, p. 640.
Chevalier, M., and Chase, B. M., 2015, Southeast African records reveal a coherent shift from high- to low-latitude forcing mechanisms along the east African margin across last glacial–interglacial transition: Quaternary Science Reviews, v. 125, p. 117-130.
Cooper, G. R. J., and Cowan, D. R., 2008, Comparing time series using wavelet-based semblance analysis: Computers & Geosciences, v. 34, no. 2, p. 95-102.
Dansgaard, W., 1964, Stable isotopes in precipitation.: Tellus, v. 16, p. 436-447.
Fischer, H., Fundel, F., Ruth, U., Twarloh, B., Wegner, A., Udisti, R., Becagli, S., Castellano, E., Morganti, A., Severi, M., Wolff, E., Littot, G., Röthlisberger, R., Mulvaney, R., Hutterli, M. A., Kaufmann, P., Federer, U., Lambert, F., Bigler, M., Hansson, M., Jonsell, U., de Angelis, M., Boutron, C., Siggaard-Andersen, M.-L., Steffensen, J. P., Barbante, C., Gaspari, V., Gabrielli, P., and Wagenbach, D., 2007, Reconstruction of millennial changes in dust emission, transport and regional sea ice coverage using the deep EPICA ice cores from the Atlantic and Indian Ocean sector of Antarctica: Earth and Planetary Science Letters, v. 260, no. 1–2, p. 340-354.
Fohlmeister, J., Voarintsoa, N. R. G., Lechleitner, F. A., Boyd, M., Brandtstätter, S., Jacobson, M. J., and L. Oster, J., 2020, Main controls on the stable carbon isotope composition of speleothems: Geochimica et Cosmochimica Acta, v. 279, p. 67-87.
Harris, C., Burgers, C., Miller, J., and Rawoot, F., 2010, O- and H-isotope record of Cape Town rainfall from 1996 to 2008, and its application to recharge studies of Table Mountain groundwater, South Africa: South African Journal of Geology, v. 113, no. 1, p. 33-56.
Herrmann, N., Boom, A., Carr, A. S., Chase, B. M., West, A. G., Zabel, M., and Schefuß, E., 2017, Hydrogen isotope fractionation of leaf wax n-alkanes in southern African soils: Organic Geochemistry, v. 109, p. 1-13.
Hijmans, R., Cameron, S. E., Parra, J. L., Jones, P. G., and Jarvis, A., 2005, Very high resolution interpolated climate surfaces for global land areas: International Journal of Climatology, v. 25, p. 1965-1978.

Holmgren, K., Lee-Thorp, J. A., Cooper, G. R. J., Lundblad, K., Partridge, T. C., Scott, L., Sithaldeen, R., Talma, A. S., and Tyson, P. D., 2003, Persistent millennial-scale climatic variability over the past 25,000 years in Southern Africa: Quaternary Science Reviews, v. 22, p. 2311-2326.

IAEA/WMO, 2020, Global Network of Isotopes in Precipitation. The GNIP Database.

Jacobs, Z., Roberts, R. G., Galbraith, R. F., Deacon, H. J., Grun, R., Mackay, A., Mitchell, P., Vogelsang, R., and Wadley, L., 2008, Ages for the Middle Stone Age of southern Africa: implications for human behavior and dispersal: Science, v. 322, no. 5902, p. 733-735.

Jouzel, J., Masson-Delmotte, V., Cattani, O., Dreyfus, G., Falourd, S., Hoffmann, G., Minster, B., Nouet, J., Barnola, J. M., Chappellaz, J., Fischer, H., Gallet, J. C., Johnsen, S., Leuenberger, M., Loulergue, L., Luethi, D., Oerter, H., Parrenin, F., Raisbeck, G., Raynaud, D., Schilt, A., Schwander, J., Selmo, E., Souchez, R., Spahni, R., Stauffer, B., Steffensen, J. P., Stenni, B., Stocker, T. F., Tison, J. L., Werner, M., and Wolff, E. W., 2007, Orbital and millennial Antarctic climate variability over the past 800,000 years.: Science, v. 317, p. 793-797.

Laskar, J., Robutel, P., Joutel, F., Gastineau, M., Correia, A. C. M., and Levrard, B., 2004, A long-term numerical solution for the insolation quantities of the Earth: A&A, v. 428, no. 1, p. 261-285.

O'Leary, M. H., 1988, Carbon isotopes in photosynthesis: Bioscience, v. 38, no. 5, p. 328-336.

Partridge, T. C., deMenocal, P. B., Lorentz, S. A., Paiker, M. J., and Vogel, J. C., 1997, Orbital forcing of climate over South Africa: a 200,000-year rainfall record from the Pretoria Saltpan: Quaternary Science Reviews, v. 16, no. 10, p. 1125-1133.

Quick, L. J., Meadows, M. E., Bateman, M. D., Kirsten, K. L., Mäusbacher, R., Haberzettl, T., and Chase, B. M., 2016, Vegetation and climate dynamics during the last glacial period in the fynbos-afrotemperate forest ecotone, southern Cape, South Africa: Quaternary International, v. 404, Part B, p. 136-149.

Rasmussen, S. O., Bigler, M., Blockley, S. P., Blunier, T., Buchardt, S. L., Clausen, H. B., Cvijanovic, I., Dahl-Jensen, D., Johnsen, S. J., Fischer, H., Gkinis, V., Guillevic, M., Hoek, W. Z., Lowe, J. J., Pedro, J. B., Popp, T., Seierstad, I. K., Steffensen, J. P., Svensson, A. M., Vallelonga, P., Vinther, B. M., Walker, M. J. C., Wheatley, J. J., and Winstrup, M., 2014, A stratigraphic framework for abrupt climatic changes during the Last Glacial period based on three synchronized Greenland ice-core records: refining and extending the INTIMATE event stratigraphy: Quaternary Science Reviews, v. 106, p. 14-28.

Rebelo, A. G., Boucher, C., Helme, N., Mucina, L., and Rutherford, M. C., 2006, Fynbos Biome, *in* Mucina, L., and Rutherford, M. C., eds., The Vegetation of South Africa, Lesotho and Swaziland: Pretoria, South African National Biodiversity Institute, p. 53-219.

Reynolds, R. W., Smith, T. M., Liu, C., Chelton, D. B., Casey, K. S., and Schlax, M. G., 2007, Daily High-Resolution-Blended Analyses for Sea Surface Temperature: Journal of Climate, v. 20, no. 22, p. 5473-5496.

Schefuß, E., Kuhlmann, H., Mollenhauer, G., Prange, M., and Pätzold, J., 2011, Forcing of wet phases in southeast Africa over the past 17,000 years: Nature, v. 480, no. 7378, p. 509-512.

Sealy, J., Lee-Thorp, J., Loftus, E., Faith, J. T., and Marean, C. W., 2016, Late Quaternary environmental change in the Southern Cape, South Africa, from stable carbon and

oxygen isotopes in faunal tooth enamel from Boomplaas Cave: Journal of Quaternary Science, v. 31, no. 8, p. 919-927.
Smith, B. N., and Epstein, S., 1971, Two categories of $^{13}C/^{12}C$ ratios for higher plants: Plant Physiology, v. 47, p. 380-384.
Talma, A. S., and Vogel, J. C., 1992, Late Quaternary paleotemperatures derived from a speleothem from Cango Caves, Cape Province, South Africa: Quaternary Research, v. 37, no. 2, p. 203-213.
Tierney, J. E., deMenocal, P. B., and Zander, P. D., 2017, A climatic context for the out-of-Africa migration: Geology, v. 45, no. 11, p. 1023-1026.
Tyson, P. D., 1986, Climatic Change and Variability in Southern Africa, Cape Town, Oxford University Press.
Vogel, J. C., 1978, Isotopic assessment of the dietary habits of ungulates: South African Journal of Science, v. 74, no. 8, p. 298-301.

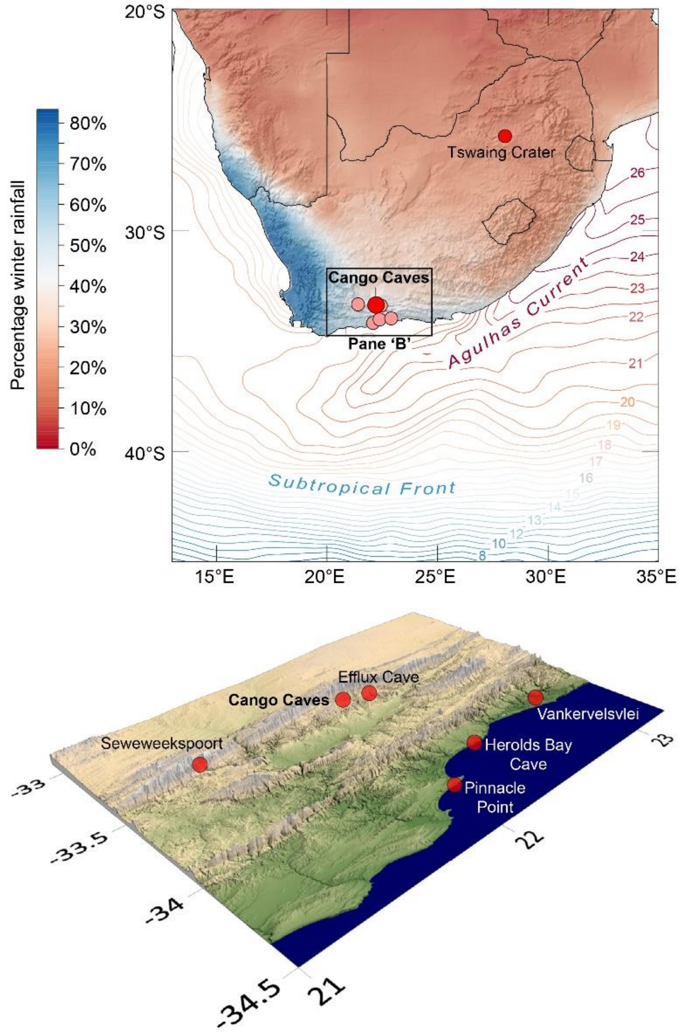

Figure 1. Map of southern Africa and study region, including sites considered and other records spanning marine isotope stage 4 and 5 from the region (Bar-Matthews et al., 2010; Braun et al., 2019; Braun et al., 2020; Chase et al., 2017; Partridge et al., 1997; Quick et al., 2016; Talma and Vogel, 1992). Map shading reflects modern rainfall seasonality (Hijmans et al., 2005) across the subcontinent provided as percentage of annual precipitation falling in winter months (here defined as April-September). Ocean contours reflect sea-surface temperatures in °C (Reynolds et al., 2007).

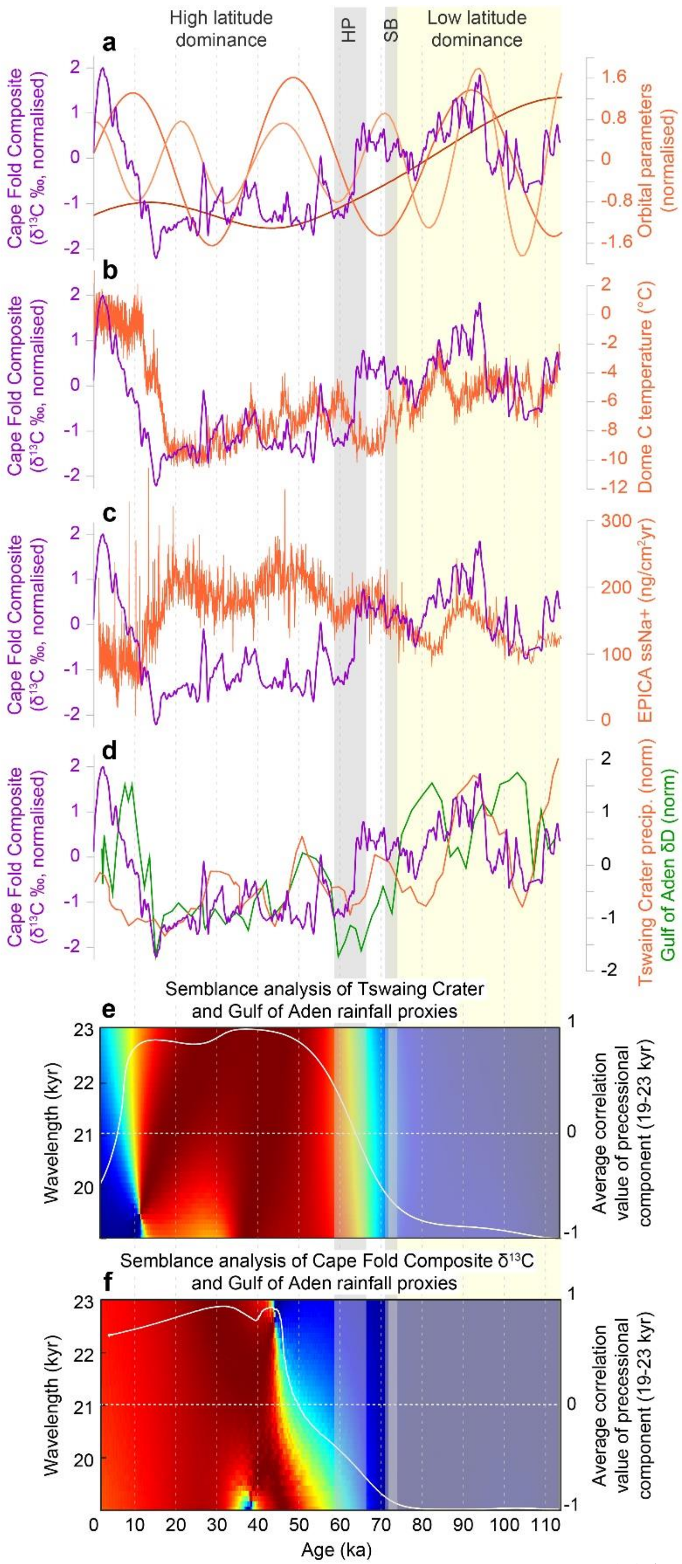

Figure 2. Comparison of the Cape Fold Composite calcite $\delta^{13}C$ record with **a)** orbital parameters (eccentricity, obliquity and summer (DJF) insolation at 25°S) (Laskar et al., 2004), **b)** the Dome C Antarctic temperature record (Jouzel et al., 2007), **c)** the Antarctic sea-salt sodium flux record (Fischer et al., 2007), and **d)** the hydroclimate proxies from Tswaing Crater, South Africa (Partridge et al., 1997) and the Gulf of Aden (δD values multiplied by -1 for comparability with Tswaing Crater record; Tierney et al., 2017). The results of semblance analyses (Cooper and Cowan, 2008; red indicates a semblance of +1 (positive correlation), and blue indicates a semblance of −1 (negative correlation)) of the precessional component of **e)** the Tswaing Crater and **f)** the Cape Fold Composite calcite $\delta^{13}C$ record and Gulf of Aden δD record indicate the transition from low to high

latitude forcing at ~70 ka. Grey shaded zones indicate the timing and duration of the Still Bay and Howiesons Poort lithic industries (Jacobs et al., 2008).

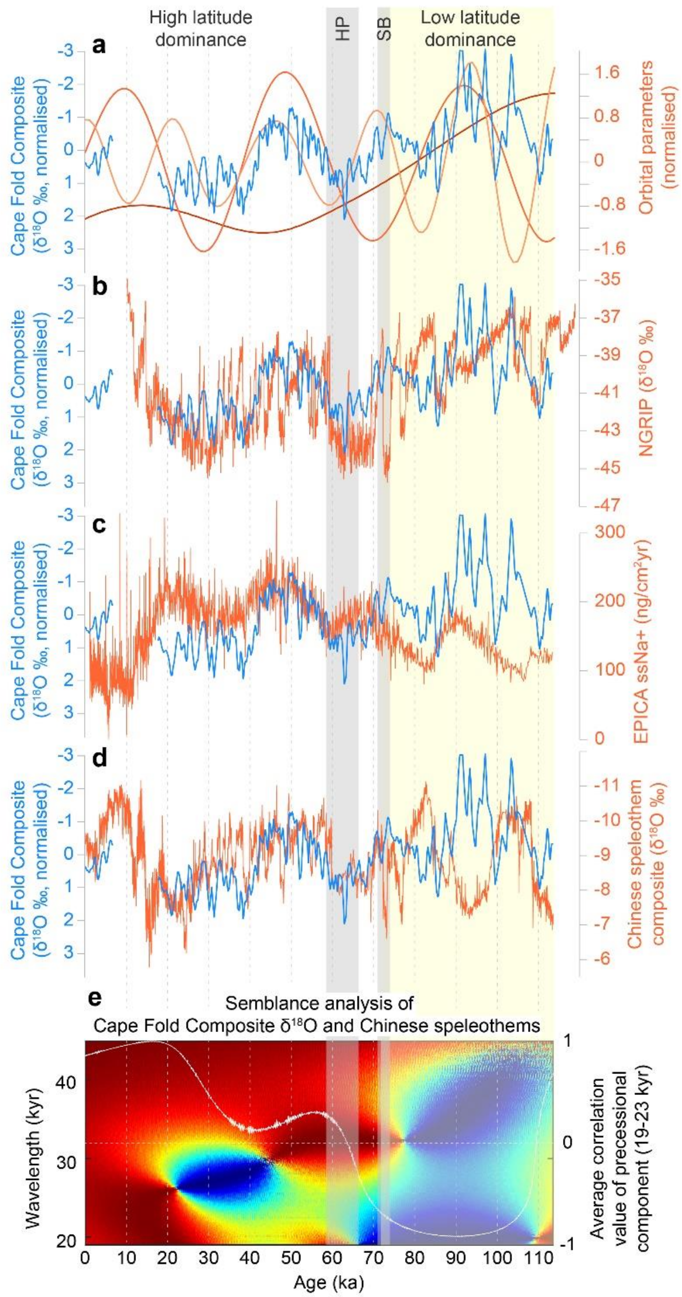

Figure 3. Comparison of the Cape Fold Composite calcite δ^{18}O record with **a)** orbital parameters (eccentricity, obliquity and summer (DJF) insolation at 25°S) (Laskar et al., 2004), **b)** the Greenland NGRIP δ^{18}O record (Rasmussen et al., 2014), **c)** the Antarctic sea-salt sodium flux record (Fischer et al., 2007), and **d)** the composite δ^{18}O record from Chinese speleothems (Cheng et al., 2016). The results of semblance analyses **(e)** (Cooper and Cowan, 2008; red indicates a semblance of +1 (positive correlation), and blue indicates a semblance of −1 (negative correlation)) of the precessional and obliquity components of Cape Fold Composite and Chinese speleothem δ^{18}O records (Cheng et al., 2016) indicate the transition from low to high latitude forcing at ~70 ka. Grey shaded zones indicate the timing and duration of the Still Bay and Howiesons Poort lithic industries (Jacobs et al., 2008).

South African speleothems reveal influence of high- and lowlatitude forcing over the past 113.5 k.y.

SUPPLEMENTARY INFORMATION

MATERIALS

The Cango Caves (33.39°S, 22.21°E) comprises a 4 km system of chambers. In 1995, a 1.55 m tall stalagmite (CAN1) was collected ~750 m from the main Cave entrance (Fig. SI1). The caves are situated in limestone that is part of the Kango Supergroup, a Neoproterozoic siliciclastic-carbonate sequence that crops out between the steep southern early Palaeozoic Table Mountain Group of the mountain range to the north, and the flat semi-arid plains of the Oudtshoorn Basin to the south, which comprises a thick, coarse terrestrial siliciclastic 'molasse' sequence of Jurassic to Cretaceous age. Earlier work on the speleothems from the Cango Caves are reported by Talma and Vogel (1992) and Vogel and Kronfeld (1997).

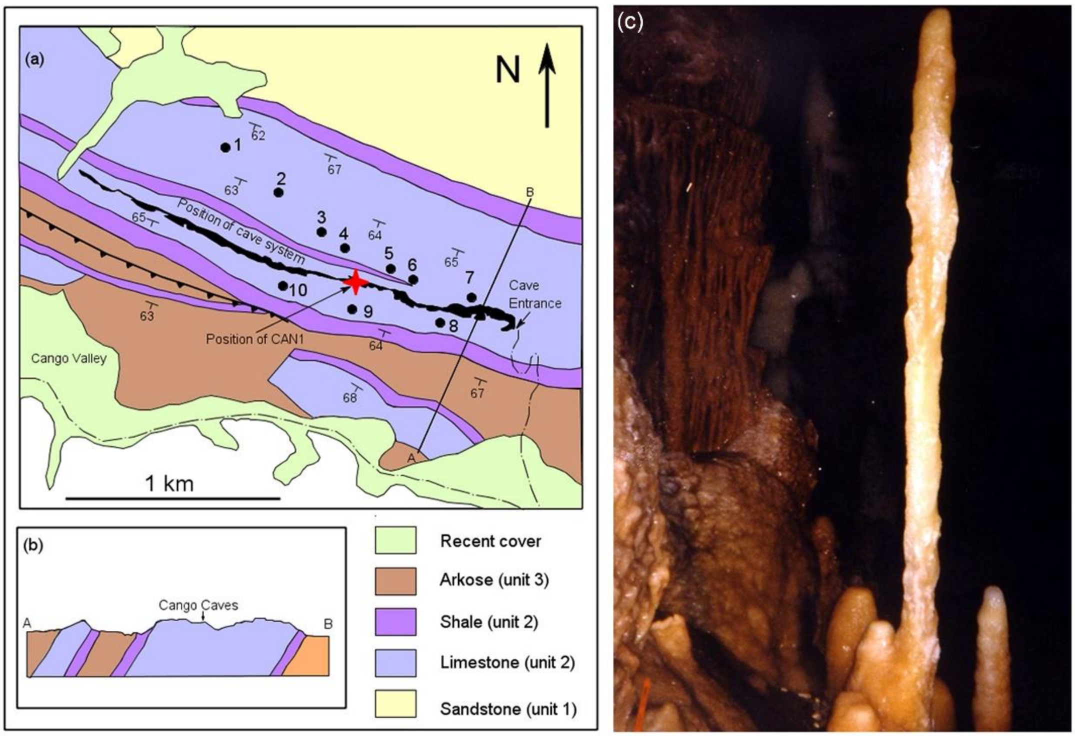

Figure SI1: Location of speleothem CAN1 in the Cango Caves system **(a)**, regional geology **(b)**, the CAN1 speleothem in-situ **(c)**. Numbers = surface rock samples (SAM prefix Table SI1). Map from Doel (1995) and cave system from South African Speleological Association (1978).

Table SI1: Surface rock sample stable carbon and oxygen isotope results. Location of samples corresponds to numbers in Figure SI1.

Country rock - Matjies River Formation				
Sample		$\delta^{13}C$	$\delta^{18}O$ SMOW	$\delta^{18}O$ PDB
SAM2		0.89	24.39	-6.32
SAM3		-4.31	25.23	-5.51
SAM4		-0.69	26.23	-4.54
SAM5		2.25	27.22	-3.58
SAM7		-0.55	26.37	-4.40
SAM8		-0.61	25.60	-5.15
SAM9		1.31	26.73	-4.05
SAM10		2.71	23.47	-7.22

METHODS

CAN1 was transported to the laboratory at the University of Cape Town and cut into six pieces of equal length and then each cut in half lengthwise using a diamond tipped rotary saw. Samples for U-series dating (n=21, 0.2-0.36 g, Table SI2) were sent to the University of Bern, Switzerland for analysis. All analysed samples come from the central axis of the stalagmite. The carbonate in CAN1 is extremely pure and no solid residue, or cloudiness in the acid, remained after dissolution in phosphoric acid.

Samples for carbon and oxygen isotope analysis (20-25 mg each) were taken every 5 cm as close as possible the central axis of each stalagmite and parallel to the growth rings, using a 2 mm drill bit. 110 samples of CAN1 were analysed at the University of Cape Town. The sampling of the CAN1 speleothem reflects the techniques of the day, and combined with the britle nature of the calcite, much of the CAN1 speleothem was destroyed in the sampling process.

Samples were analysed using both off-line and standard gas-bench techniques. Off-line extraction of CO_2 from carbonates was made using the method of McCrea (1950) with 100% phosphoric acid. Samples were reacted at 25°C and a CO_2-calcite fractionation factor of 1.01025 was used to correct the raw data. C and O isotope ratios were measured using either a Finnegan MAT252 or a Thermo XP mass spectrometer. An internal calcite standard (NM; $\delta^{13}C$ = 1.57‰, $\delta^{18}O$ = 25.10‰ relative to PDB and SMOW, respectively) calibrated using NBS-19 was used to normalize raw data to the SMOW and PDB scales. Repeat analysis of the NM standard suggests that the precision is 0.2 and 0.1‰ for $\delta^{18}O$ and $\delta^{13}C$, respectively. Samples were reacted at 70˚C using the on-line gas bench analysed along with the standards Lincoln Limestone, NBS18 and NBS20, which have a range of $\delta^{13}C$ and $\delta^{18}O$ values. The measured and accepted values were used to construct a calibration curve and this was used to correct the raw data, and to determine the precision of the method. Repeated analyses of the standards suggest that the $\delta^{13}C$ and $\delta^{18}O$ values are accurate to within 0.14‰ and 0.18‰ (2σ), respectively.

RESULTS
Uranium-series dating and age model development

Table. SI2: Cango Caves speleothem U-series dating results. Activity ratios calculated using the decay constants for ^{234}U and ^{230}Th determined by Cheng et al. (2013). Values/yr: ^{234}U (2.8222 ± 0.0030)E-6 and ^{230}Th (9.1706 ± 0.01335)E-6. For samples with significant Th/U ratios (Table B), corrections applied in Table A are based on the assumption that the "detrital fraction" has a Th/U ratio similar to that of average continental crust (4.2) and has U-series nuclides in secular equilibrium. Detrital fractions rarely have Th/U ratios lower than 4.2, and these corrections are the maximum to be expected.

TABLE A				**Activity ratios**									
Sample name	**Dist, mm**	**ppb U**	**ppb Th**	**($^{230}Th/^{238}U$)**	**± 1SE**	**($^{234}U/^{238}U$)**	**± 1SE**	**($^{230}Th/^{234}U$)**	**± 1SE**	**App. Age (ka)**	**± 95%**	**($^{234}U/^{238}U$) init.**	**± 95%**
CAN 1- 1	0	68.7	7.4	1.174	0.001	3.006	0.015	0.391	0.003	**38.7**	0.9	3.24	0.03
CAN 1- 3	100	76.8	2.6	1.389	0.001	3.097	0.005	0.448	0.004	**60.3**	1.3	3.49	0.02
CAN 1- 6 R	250	40.6	0.8	1.351	0.002	2.640	0.009	0.512	0.004	**71.5**	1.7	3.01	0.02
CAN 1- 7	300	44.0	3.4	1.474	0.009	2.654	0.006	0.556	0.024	**80.3**	9.3	3.08	0.06
CAN 1- 8	350	36.2	2.3	1.489	0.003	2.688	0.006	0.554	0.007	**79.9**	2.8	3.12	0.02
CAN 1- 9 R	400	39.5	0.5	1.516	0.002	2.814	0.007	0.539	0.005	**76.5**	1.8	3.25	0.02
K 9	400	48.5	n.d	1.453	0.005	2.697	0.006	0.539	0.003	**77.0**	1.4	3.11	0.01
CAN 1- 12	550	27.3	0.3	1.572	0.003	2.692	0.016	0.584	0.007	**85.8**	2.9	3.16	0.04
CAN 1- 15 R	700	54.6	0.2	1.560	0.002	2.661	0.007	0.586	0.005	**86.4**	1.8	3.12	0.02
CAN 1-15 B	722	55.3	10.0	1.688	0.012	2.715	0.007	0.622	0.005	**93.8**	2.1	3.23	0.02
CAN 1-16	750	56.3	4.4	1.685	0.012	2.700	0.004	0.624	0.004	**94.3**	1.7	3.22	0.02
CAN 1-17 B	819	42.7	0.5	1.709	0.012	2.717	0.011	0.629	0.005	**95.1**	2.2	3.25	0.03
CAN 1-17 D	840	50.0	0.8	1.744	0.012	2.727	0.003	0.639	0.004	**97.2**	2.0	3.27	0.02
CAN 1-18	850	59.6	1.2	1.698	0.013	2.671	0.005	0.636	0.005	**96.5**	2.2	3.20	0.02
CAN 1-18 B	876.5	58.4	1.0	1.709	0.012	2.650	0.006	0.645	0.005	**98.8**	2.2	3.18	0.02
CAN 1-19 A	913	53.0	0.9	1.785	0.013	2.751	0.005	0.649	0.005	**99.4**	2.2	3.32	0.02
CAN 1- 22 R	1050	56.7	0.6	1.726	0.002	2.727	0.005	0.633	0.005	**96.0**	2.0	3.27	0.02
K 22	1050	62.1	n.d.	1.600	0.005	2.583	0.006	0.620	0.003	**93.3**	1.1	3.06	0.01
CAN 1- 24 R	1150	71.3	0.1	1.727	0.002	2.765	0.004	0.625	0.005	**94.4**	2.0	3.30	0.02
K 28	1350	59.1	n.d.	1.746	0.006	2.698	0.008	0.647	0.004	**99.1**	1.3	3.25	0.02
K 31	1500	67.2	n.d.	1.821	0.006	2.712	0.007	0.671	0.004	**104.6**	1.3	3.30	0.01

Table. SI2 cont'd: Cango Caves speleothem U-series dating results. Activity ratios calculated using the decay constants for ^{234}U and ^{230}Th determined by Cheng et al. (2013). Values/yr: ^{234}U (2.8222 ± 0.0030)E-6 and ^{230}Th (9.1706 ± 0.01335)E-6. For samples with significant Th/U ratios (Table B), corrections applied in Table A are based on the assumption that the "detrital fraction" has a Th/U ratio similar to that of average continental crust (4.2) and has U-series nuclides in secular equilibrium. Detrital fractions rarely have Th/U ratios lower than 4.2, and these corrections are the maximum to be expected.

TABLE B				**atomic**		**Activity ratios**			
Sample name	**Dist, mm**	**ppb U**	**ppb Th**	**232Th/238U**	**238U Fr detrital**	**($^{230}Th/^{238}U$)**	**± 1SE**	**($^{234}U/^{238}U$)**	**± 1SE**
CAN 1- 1	0	68.7	7.4	0.111	0.0278	1.169	0.001	2.950	0.015
CAN 1-3	100	76.8	2.6	0.034	0.0086	1.385	0.001	3.079	0.005
CAN 1- 7	300	44.0	3.4	0.079	0.0197	1.465	0.009	2.621	0.006
CAN 1-8	350	36.2	2.3	0.066	0.0164	1.481	0.003	2.660	0.006
CAN 1-15 B	722	55.3	10.0	0.187	0.0466	1.656	0.012	2.635	0.007
CAN 1-16	750	56.3	4.4	0.082	0.0204	1.671	0.012	2.665	0.004

U/Th ages (Table SI2) from CAN1 ranged from 38.7±0.9 ka (0 mm) to 104.6±1.3 ka (at 1500 mm). Some age reversals do exist, and a Bayesian technique (rbacon v.2.4.3; Blaauw and Christen, 2011) was used to create an age model that incorporated all of the available data (Fig. SI2).

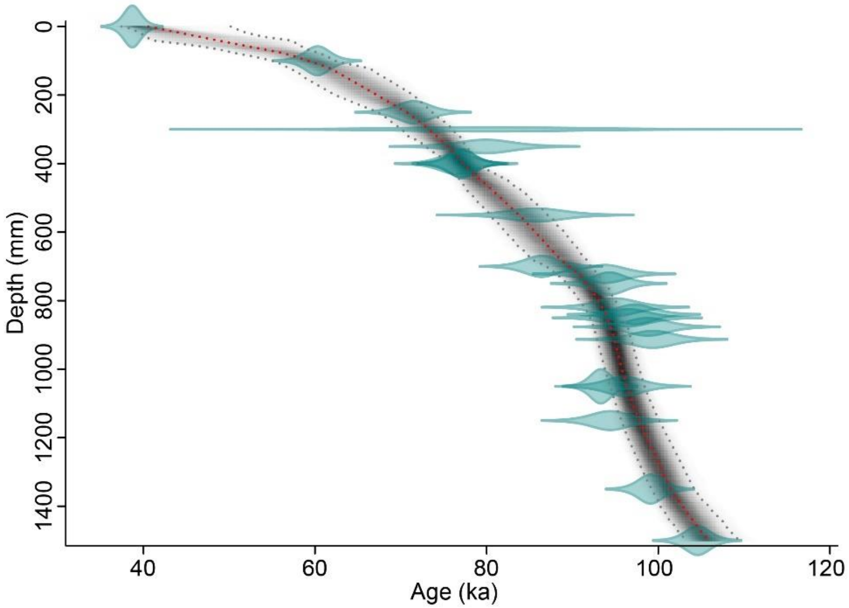

Figure. SI2: Speleothem CAN1 age-depth model, established using rbacon v.2.4.3 (Blaauw and Christen, 2011).

Isotopic equilibrium

The $\delta^{18}O$ values of authigenic carbonate depend on the temperature of precipitation in the cave and the $\delta^{18}O$ value of the water from which the calcite precipitates. It is also important that isotope equilibrium be maintained. In cases where the correlation between $\delta^{13}C$ and $\delta^{18}O$ values is significant, it is probably due to kinetic effects related to evaporation, and there is limited relationship between temperature and $\delta^{18}O$ value. This situation is typical in carbonate taken from the flanks of speleothems (Hendy, 1971). For CAN1, there is no correlation between $\delta^{13}C$ and $\delta^{18}O$ values (Fig. SI3), which is consistent with precipitation of calcite in isotope equilibrium.

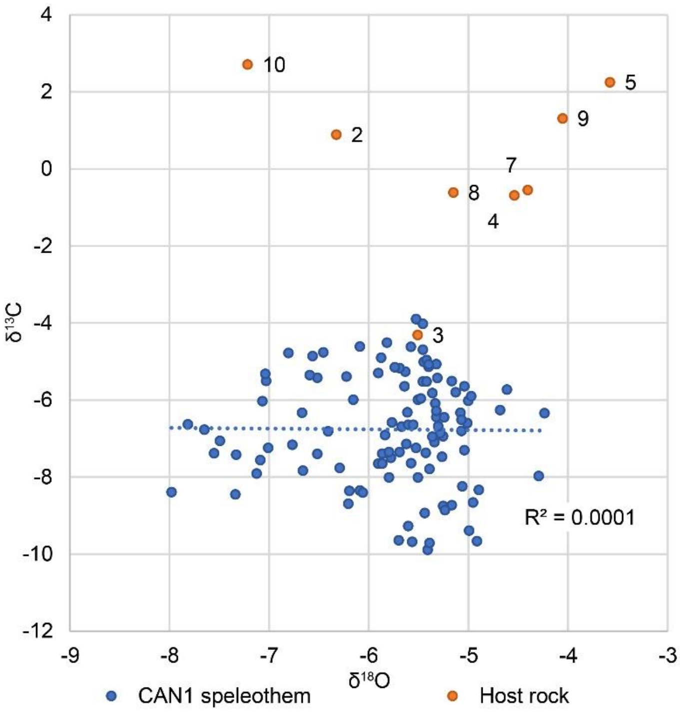

Figure. SI3: Speleothem CAN1 calcite and host rock $\delta^{13}C$ and $\delta^{18}O$ values. Lack of correlation between CAN1 $\delta^{13}C$ and $\delta^{18}O$ indicates the calcite precipitated in isotopic equilibrium.

The $\delta^{13}C$ and $\delta^{18}O$ values and composite model development

The $\delta^{13}C$ values of the samples (n=112) vary between -3.9‰ and -9.89‰, and the $\delta^{18}O$ between -4.24‰ and -7.98‰ relative to the Vienna PeeDee Belemnite (VPDB) standard (Fig SI4). Kinetic fractionation during crystallization of calcite leads to strong correlation between $\delta^{13}C$ and $\delta^{18}O$ values, and it is clear that no such correlation exists (Fig SI3). Whereas the $\delta^{13}C$ values from CAN1 exhibit a high signal-to-noise ratio, the $\delta^{18}O$ values are more variable, and were smoothed using a 3-point moving average to reduce noise.

To maximise the utility of the CAN1 data and their integration into the aggregate regional dataset, the data were used as the basis for the creation of composite records integrating comparable data from Efflux Cave (Braun et al., 2020), previously published data from the Cango Caves (Talma and Vogel, 1992) and, in the case of the $\delta^{13}C$ data, data from the Seweweekspoort rock hyrax middens (Chase et al., 2017). The composite records (referred to hereafter as Cape Fold Composites; CFC) were created to obtain a coherent signal from the aggregated data (Fig. SI5, 6).

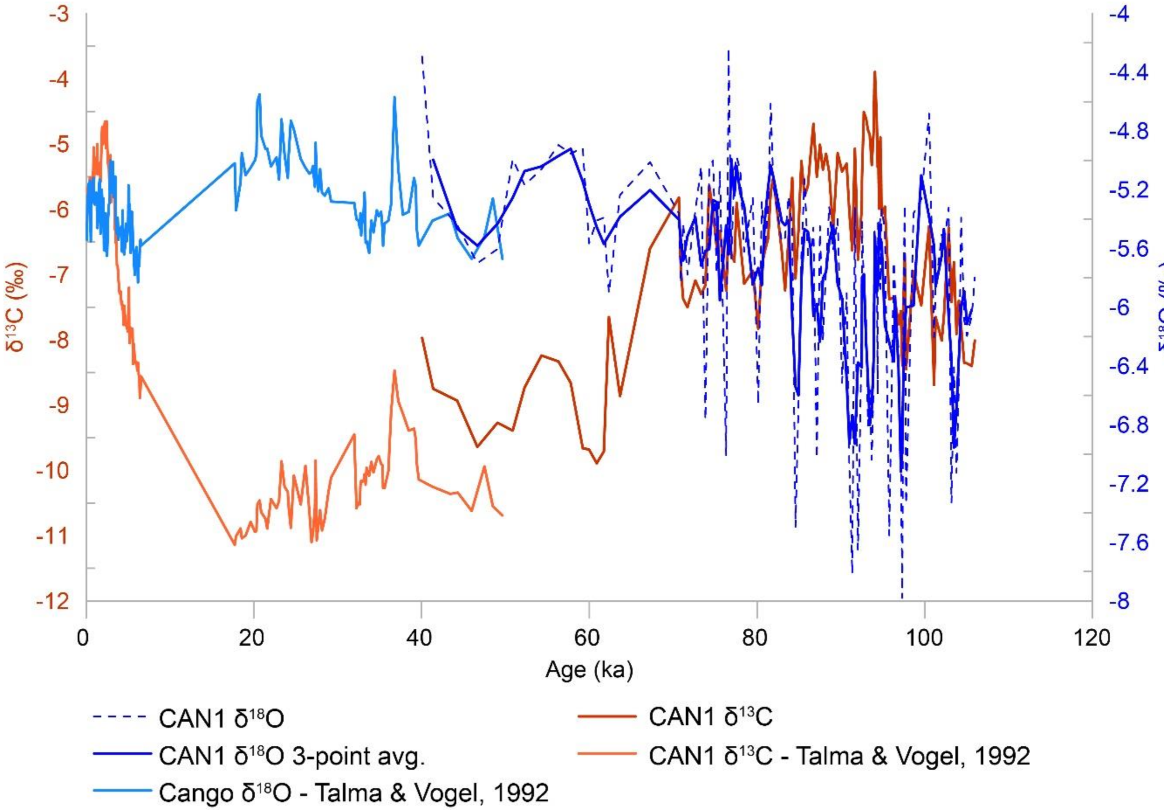

Figure. SI4: Oxygen and carbon isotope records from the Cango Caves, including the CAN1 data presented in this paper and the data of Talma and Vogel (1992).

The speleothem $\delta^{13}C$ records reflect changes in the vegetation specific to each site/record, including the potential presence of micro-scale vegetation mosaics that may result in significant differences in the $\delta^{13}C$ content of individual speleothems from the same cave, as is the case in Efflux Cave (Braun et al., 2020). It is important to note that while individual speleothem $\delta^{13}C$ contents may differ, and the amplitudes of the signals expressed may vary (both as a function of the vegetation present in the drip water source locale), the sign of the signal – reflecting the changes in climate that drive vegetation response – is generally consistent between the records considered here, indicating that a climate signal can be derived from the data. To accurately define this signal at the regional scale, it is necessary to apply scaling transformations to individual records. The Cango Caves speleothems indicate similar $\delta^{13}C$ values and amplitudes, and, based on the difference of the mean values of the overlapping portions, a simple x-1.1968 transformation was applied to the CAN1 $\delta^{13}C$ record to align it with the Cango Caves speleothem $\delta^{13}C$ record of Talma and Vogel (1992), creating a Cango Caves composite $\delta^{13}C$ record. To account for regional differences in vegetation composition, and render the Efflux Cave $\delta^{13}C$ records comparable both with each other and with the Cango Caves composite record, reduced major axis regression (RMA) was used between each of the Efflux Cave speleothem $\delta^{13}C$ records and the overlapping section of the Cango Caves composite $\delta^{13}C$ record to estimate scaling transformations to minimize the Euclidean distance between the datasets (for speleothem 142843, (x*0.39647)-6.9412; for speleothem 142848, (x*1.354)-4.9988; speleothems 142847 and 142849 were combined prior to scaling to improve overlap with Cango Caves composite, (x*0.74706)-4.1018; speleothem 142846 does not overlap with any other record, but based on similarities in value and amplitude of variability with speleothems 142847 and 142849 the same (x*0.74706)-4.1018 transform was applied). Based on the similarities between the Cango Caves speleothem $\delta^{13}C$ record of Talma and Vogel (1992) and the Seweweekspoort rock hyrax midden $\delta^{13}C$ record (Chase et al., 2017), we have used this latter record to span the hiatus present in the Talma and Vogel record. As with the Efflux Cave data, RMA regression between the Seweweekspoort $\delta^{13}C$ record and the Cango Caves composite $\delta^{13}C$ record was used to estimate a scaling transformation ((x*1.642)+33.94) for the Seweweekspoort data. Finally, the Cango Caves, Efflux Cave and Seweweekspoort records were compiled, sorted by age, normalized using a standard score (to avoid confusion regarding reporting of corrected $\delta^{13}C$ data) and, to improve the signal to noise ratio (Fig. SI5).

The speleothem $\delta^{18}O$ records were combined to create a composite record using the same process that was applied to the $\delta^{13}C$ records, with the same goal of obtaining a record that reflects regional changes in climate with a high signal to noise ratio. As the CAN1 $\delta^{18}O$ record expresses particularly high frequency variability prior to ~70 ka (likely a product of the increase in tropical influence described in the main text) a 3-point moving average was applied as an initial step to improve the signal to noise ratio. The CAN1 speleothem and that analysed by Talma and Vogel (1992) indicate similar $\delta^{18}O$ values and amplitudes for the 40-50 ka period during which they overlap, and the records were simply compiled and sorted by age and normalized using a standard score to obtain a composite record. Determined by similarities in terms of values and amplitudes of variability between Efflux Cave speleothem $\delta^{18}O$ records 142843, 142846, 142847 and 142849 were compiled and sorted by age, to create a partial composite. The $\delta^{18}O$ record from speleothem 142848 exhibits a pattern of overall variability similar to the other Efflux Cave $\delta^{18}O$ records, but at slightly higher values and reduced amplitude of variability. RMA regression was used to estimate a scaling transformation ((x*2.3855)+4.9234) to minimize the Euclidean distance between the 142848 $\delta^{18}O$ record and the Efflux Cave partial composite. With this transformation applied, the 142848 $\delta^{18}O$ record was compiled with the other Efflux Cave $\delta^{18}O$ records, and the aggregate was sorted by age and normalized using a standard score. RMA regression was then applied to the overlapping sections of the Cango Caves and Efflux Cave composite $\delta^{18}O$ records, with a scaling transform of (x*0.61024)+0.16217 being applied to the Efflux Cave composite to create a coherent regional CFC composite $\delta^{18}O$ record (Fig. SI6).

Both the CFC $\delta^{13}C$ and $\delta^{18}O$ records were smoothed using a Gaussian kernel method with a kernel width sigma = 0.3 ka. These composites are plotted with 95% confidence intervals for the reconstructions in Fig. SI5,6. Uncertainties associated with age estimates are indicated in Table SI2 and the original papers describing the Efflux Cave speleothems (Braun et al., 2020) and the speleothem from the Cango Caves analysed by Talma and Vogel (1992; Vogel and Kronfeld, 1997).

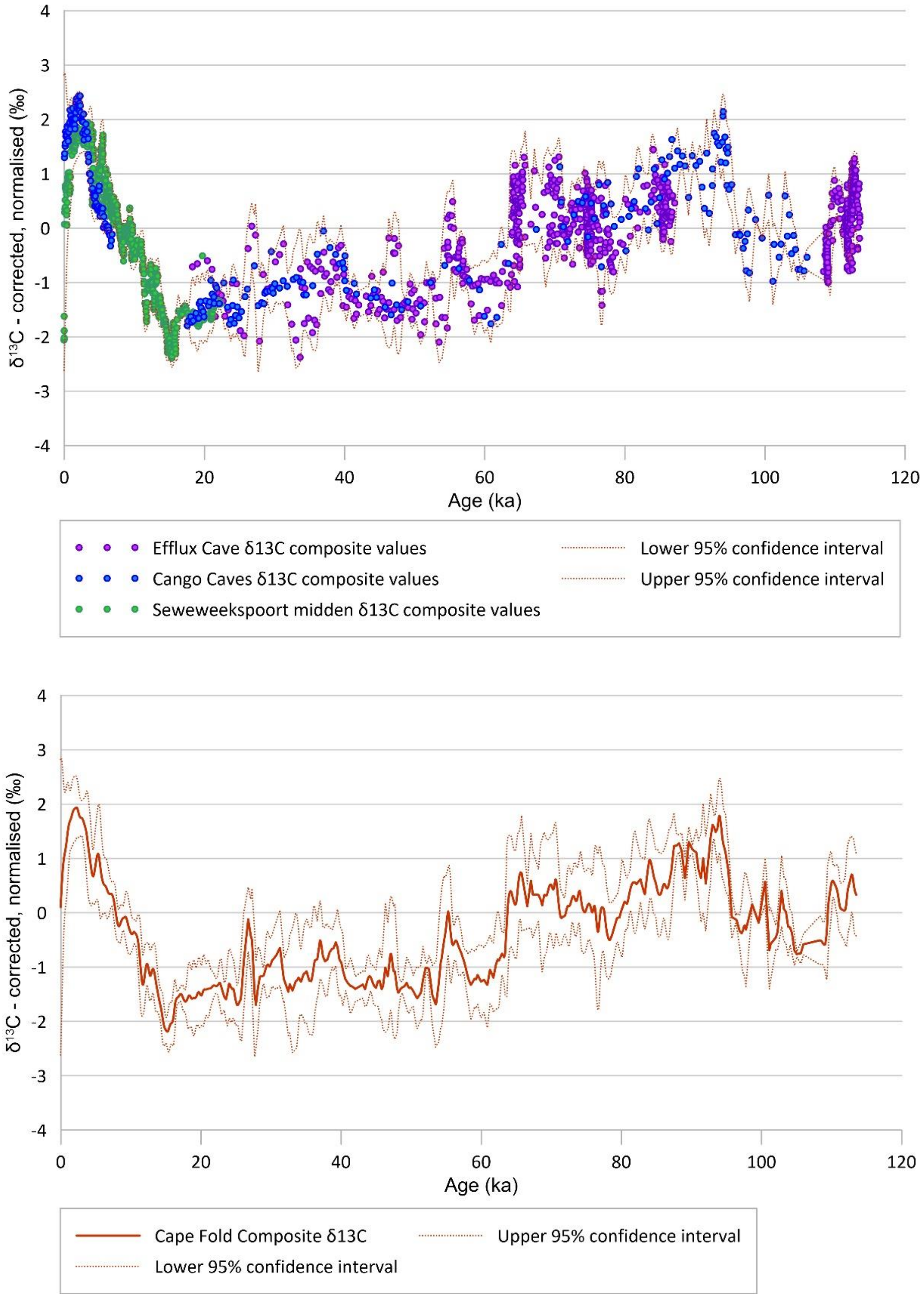

Figure. SI5: Cape Fold Composite $\delta^{13}C$ record: Component and composite stable carbon isotope records from the Cango Caves - CAN1 and the data of Talma and Vogel (1992), Efflux Cave (Bar-Matthews et al., 2010; Braun et al., 2020), and the Seweweekspoort rock hyrax middens (Chase et al., 2017). Composite records and 95% confidence intervals for the composite were established using a Gaussian kernel method with a kernel width sigma = 0.3 ka.

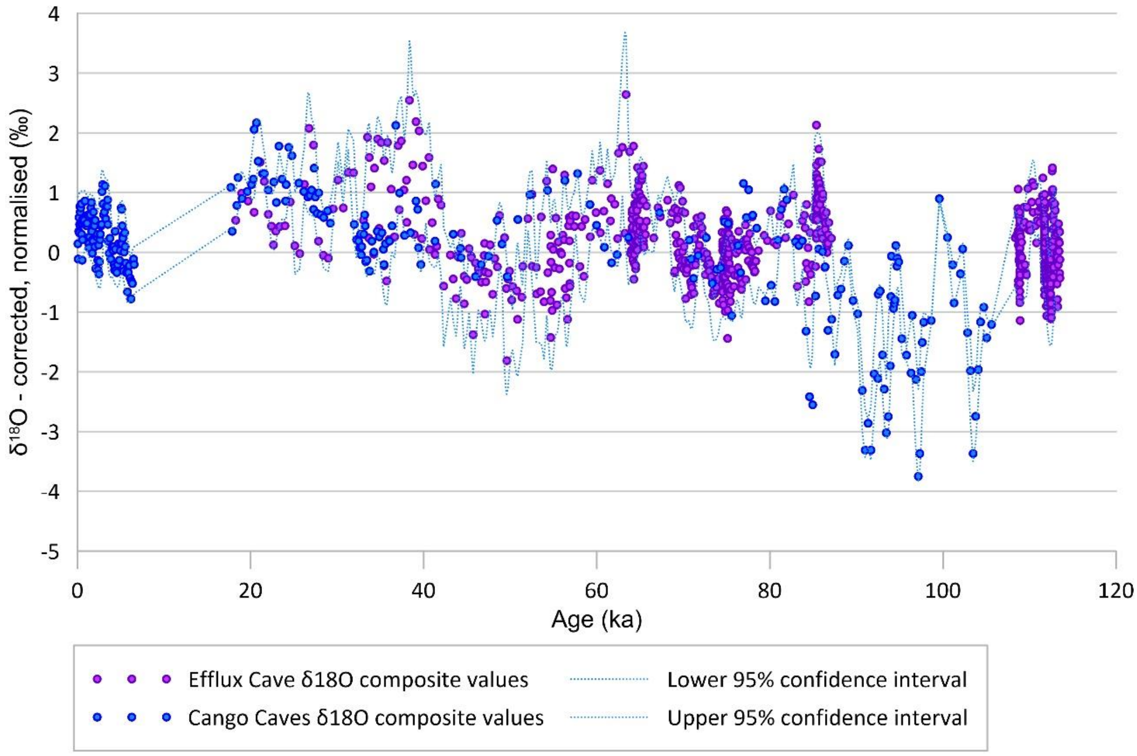

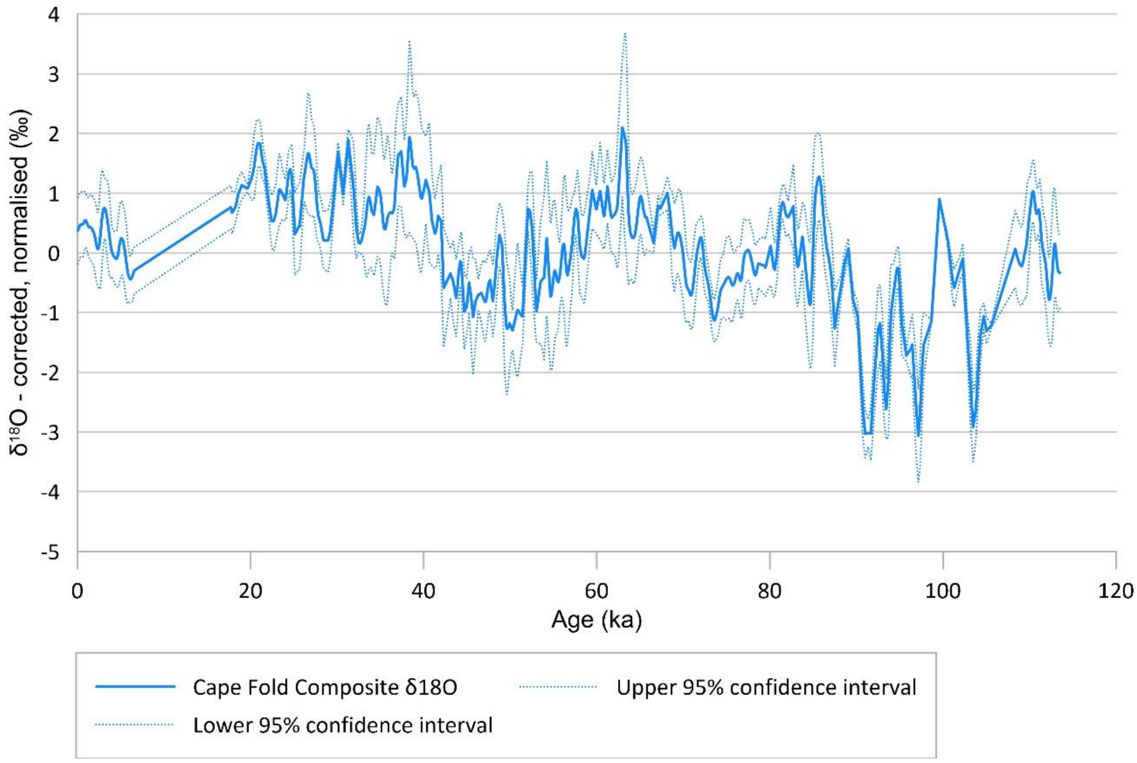

Figure. SI6: Cape Fold Composite $\delta^{18}O$ record: Component and composite stable oxygen isotope records from the Cango Caves - CAN1 and the data of Talma and Vogel (1992) - and Efflux Cave (Bar-Matthews et al., 2010; Braun et al., 2020). Composite records and 95% confidence intervals for the composite were established using a Gaussian kernel method with a kernel width sigma = 0.3 ka.

REFERENCES

South African Spelaeological Association, 1978, Cango Cave - The combined 1956 & 1978 surveys by the S.A. Spelaeological Association (Cape Section).

Bar-Matthews, M., Marean, C. W., Jacobs, Z., Karkanas, P., Fisher, E. C., Herries, A. I. R., Brown, K., Williams, H. M., Bernatchez, J., Ayalon, A., and Nilssen, P. J., 2010, A high resolution and continuous isotopic speleothem record of paleoclimate and paleoenvironment from 90 to 53 ka from Pinnacle Point on the south coast of South Africa: Quaternary Science Reviews, v. 29, no. 17-18, p. 2131-2145.

Blaauw, M., and Christen, J. A., 2011, Flexible paleoclimate age-depth models using an autoregressive gamma process: Bayesian Analysis, v. 6, no. 3, p. 457-474.

Braun, K., Bar-Matthews, M., Matthews, A., Ayalon, A., Zilberman, T., Cowling, R. M., Fisher, E. C., Herries, A. I. R., Brink, J. S., and Marean, C. W., 2020, Comparison of climate and environment on the edge of the Palaeo-Agulhas Plain to the Little Karoo (South Africa) in Marine Isotope Stages 5–3 as indicated by speleothems: Quaternary Science Reviews, v. 235, p. 105803.

Chase, B. M., Chevalier, M., Boom, A., and Carr, A. S., 2017, The dynamic relationship between temperate and tropical circulation systems across South Africa since the last glacial maximum: Quaternary Science Reviews, v. 174, p. 54-62.

Cheng, H., Lawrence Edwards, R., Shen, C.-C., Polyak, V. J., Asmerom, Y., Woodhead, J., Hellstrom, J., Wang, Y., Kong, X., Spötl, C., Wang, X., and Calvin Alexander, E., 2013, Improvements in 230Th dating, 230Th and 234U half-life values, and U–Th isotopic measurements by multi-collector inductively coupled plasma mass spectrometry: Earth and Planetary Science Letters, v. 371-372, p. 82-91.

Doel, S. L., 1995, Cango Caves stable isotope stratigraphy [BSc Honours: University of Cape Town.

Hendy, C. H., 1971, The isotopic geochemistry of speleothems--I. The calculation of the effects of different modes of formation on the isotopic composition of speleothems and their applicability as palaeoclimatic indicators: Geochimica et Cosmochimica Acta, v. 35, no. 8, p. 801-824.

Talma, A. S., and Vogel, J. C., 1992, Late Quaternary paleotemperatures derived from a speleothem from Cango Caves, Cape Province, South Africa: Quaternary Research, v. 37, no. 2, p. 203-213.

Vogel, J. C., and Kronfeld, J., 1997, Calibration of radiocarbon dates for the Late Pleistocene using U/Th dates on stalagmites: Radiocarbon, v. 39, no. 1, p. 27-32.